

# A Non-Local Means Filter for Removing the Poisson Noise

Qiyu JIN · Ion Grama · Quansheng Liu

the date of receipt and acceptance should be inserted later

**Abstract** A new image denoising algorithm to deal with the Poisson noise model is given, which is based on the idea of Non-Local Mean. By using the "Oracle" concept, we establish a theorem to show that the Non-Local Means Filter can effectively deal with Poisson noise with some modification. Under the theoretical result, we construct our new algorithm called Non-Local Means Poisson Filter and demonstrate in theory that the filter converges at the usual optimal rate. The filter is as simple as the classic Non-Local Means and the simulation results show that our filter is very competitive.

**Keywords** Non-Local Means · Mean Square Error · Poisson noise · "Oracle" estimator

---

Qiyu JIN

Institute of Image Processing and Pattern Recognition, Shanghai Jiao Tong University, No. 800 Dongchuan Road, Minhang District, Shanghai 200240, China

UMR 6205, Laboratoire de Mathématiques de Bretagne Atlantique, Université de Bretagne-Sud, Campus de Tohaninic, BP 573, 56017 Vannes, France

Université Européenne de Bretagne, France

Jiangsu Engineering Center of Network Monitoring, Nanjing University of Information Science & Technology, Nanjing 210044, China

E-mail: qiyu.jin2008@gmail.com

Ion Grama

UMR 6205, Laboratoire de Mathématiques de Bretagne Atlantique, Université de Bretagne-Sud, Campus de Tohaninic, BP 573, 56017 Vannes, France

Université Européenne de Bretagne, France

E-mail: ion.grama@univ-ubs.fr

Quansheng Liu

UMR 6205, Laboratoire de Mathématiques de Bretagne Atlantique, Université de Bretagne-Sud, Campus de Tohaninic, BP 573, 56017 Vannes, France

Université Européenne de Bretagne, France

School of Mathematics and Computing Sciences, Changsha University of Science and Technology, Changsha 410076, China

E-mail: quansheng.liu@univ-ubs.fr

## 1 Introduction

Noise is inevitable in any image device. A digital imaging system consists of an optical system followed by a photodetector and associated electrical filters. The photodetector converts the incident optical intensity to a detector current, i.e. photons to electrons. During the process, the true signals are contaminated by many different sources of noise. The Poisson noise appears in low-light conditions when the number of collected photons is small, such as night vision, medical imaging, underwater imaging, microscopic imaging, optical microscopy imaging and astronomy imaging. Such a noise is signal-dependent, and requires to adapt the usual denoising approaches.

The key challenge in Poisson intensity estimation problems is that the variances of the observed counts are different. As a result, many methods are introduced to transform the Poisson distributed noise to the data approximately Gaussian and homoscedastic. These methods are called Variance Stabilizing Transformations (VST), such as Anscombe root transformation (1948 [4], and 1993 [6]), multiscale VSTs (2008 [39]), conditional variance stabilization (CVS) (2006 [18]), or Haar-Fisz transformation (2004 [15] and 2007 [14]). Then we can deal with these data as Gaussian noise. Second, the noise is removed using a conventional denoising algorithm for additive white Gaussian noise, see for example Buades, Coll and Morel (2005 [8]), Kervrann (2006 [22]), Aharon and Elad and Bruckstein (2006 [2]), Hammond and Simoncelli (2008 [16]), Polzehl and Spokoiny (2006 [34]), Hirakawa and Parks (2006 [17]), Mairal, Sapiro and Elad (2008 [27]), Portilla, Strela, Wainwright and Simoncelli (2003 [35]), Roth and Black (2009 [36]), Katkovnik, Foi, Egiazarian, and Astola (2010 [21]), Dabov, Foi, Katkovnik and Egiazarian (2006 [9]), Abraham, Abraham, Desolneux and Li-Thiao-Te (2007 [1]), and Jin, Grama and Liu (2011 [20]). After denoising, some inverse transformations, like Exact Unbiased Inverse (EUI) (2009 [28] and 2011 [29]), are applied to the denoised signal, obtaining the estimate of the signal of interest. Many authors restore the Poisson noise by this type of methods with a three-step procedure (see [7, 25, 26, 39]).

Maximum Likelihood (ML) estimation (1996 [38], 2009[32]) and Similarity Measure (SM) (2006 [3]) are also found to be effective since they can account for the special properties of the Poisson distribution. Other methods like as Complexity-Penalized Likelihood Estimation (CPL) (2000 [33], 2005 [23]) and Total Variation (TV) seminorm (2009 [5]), have been introduced to deal with the Poisson noise. Le et al. ([24]) have adapted the successful ROF model for total variation regularization to deal with Poisson noise. The gradient descent iteration for this model replaces the regularization parameter with a function.

The Non-Local Means Filter has been proposed by Buades *et al* (2005 [8]) to denoise images damaged by additive white Gaussian noise. It is based on the similarity phenomenon existing very often in natural images, and assumes that there is enough redundant information (pixels having identical noise-free value) in the image to reduce the noise significantly. This filter is known to efficiently reduce the noise and to preserve structures. Some authors (see 2008

[7], 2010 [10]) combine the Non-Local Means method with other methods to restore the Poisson noise. Deledalle et al. (2010 [10]) proposed an extension of the Non-Local Means for images damaged by Poisson noise. It is based on probabilistic similarities to compare noisy patches and patches of a pre-estimated image.

In this paper, a new image denoising algorithm to deal with the Poisson noise model is given, which is based on the idea of Non-Local Mean. Our main idea is as follows: we first obtain an "Oracle" estimator by minimized a very tight upper bound of the Mean Square Error with changing the size of search window. The "Oracle" estimator depends on the unknown target function (original image), whose concept is developed in Donoho and Johnstone [11]. So the "Oracle" estimator is not computable, but it can help us to find an available algorithm in mathematic theory. We second establish a theorem by the concept of the "Oracle" to show that the Non-Local Means Filter can effectively deal with Poisson noise with some modification. Finally, replacing the unknown target function by some estimators, we construct our new algorithm called Non-Local Means Poisson Filter and demonstrate in statistic theory that the filter converges at the usual optimal rate. The filter is as simple as the classic Non-Local Means and the simulation results show that our filter is very competitive.

The remainder of this paper is organized as follow: we first introduce an "Oracle" estimator for Poisson noise based on the idea of Non-Local Means, and present a theorem to show the rate of convergence of the "Oracle" estimator in Section 2. We second construct an adaptive estimator according to the "Oracle" estimator and obtain some convergence theorems of the estimator in Section 3. Finally, we demonstrate in Section 4 the ability of approach at restoring image contaminated by Poisson noise with a brief analysis.

## 2 The "Oracle" estimator

### 2.1 Some notations

We suppose that the original image of the object being photographed is a integrable two-dimensional function  $f(x)$ ,  $x \in (0, 1] \times (0, 1]$ . Let the mean value of  $f$  in a set  $\mathbf{B}_x$  be

$$\Lambda(\mathbf{B}_x) = N^2 \int_{\mathbf{B}_x} f(t) dt.$$

Typically we observe a discrete dataset of counts  $\mathbf{Y} = \{\mathcal{N}(\mathbf{B}_x)\}$ , where  $\mathcal{N}(\mathbf{B}_x)$  is a Poisson random variable of intensity  $\Lambda(\mathbf{B}_x)$ . We consider that if  $\mathbf{B}_x \cap \mathbf{B}_y = \emptyset$ , then  $\mathcal{N}(\mathbf{B}_x)$  is independent of  $\mathcal{N}(\mathbf{B}_y)$ . Suppose that  $x = (x^{(1)}, x^{(2)}) \in \mathbf{I} = \{\frac{1}{N}, \frac{1}{N}, \dots, 1\}^2$ , and  $\mathbf{B}_x = (x^{(1)} - 1/N, x^{(1)}] \times (x^{(2)} - 1/N, x^{(2)}]$ . Then  $\{\mathbf{B}_x\}_{x \in \mathbf{I}}$  is a partition of the square  $(0, 1] \times (0, 1]$ . Using this partition we get a discrete function  $f(x) = \Lambda(\mathbf{B}_x)$ ,  $x \in \mathbf{I}$ . The denoising algorithm aims

at estimating the underlying intensity profile discrete function  $f(x) = A(\mathbf{B}_x)$ . The image function  $f$  is considered to be constant on each  $\mathbf{B}_x$ ,  $x \in \mathbf{I}$ . Therefore  $f(x) = \mathcal{N}(\mathbf{B}_x)$ ,  $x \in \mathbf{I}$ . Furthermore, we can estimate the integrable function  $p$  by the discrete function  $f$ . Let

$$Y(x) = \mathcal{N}(\mathbf{B}_x), \quad x \in \mathbf{I}. \quad (1)$$

This model has been used effectively in many contexts. The Poisson noise model can be rewritten in the regression form

$$Y(x) = f(x) + \epsilon(x), \quad x \in \mathbf{I}, \quad (2)$$

where  $\epsilon(x) = \mathcal{N}(\mathbf{B}_x) - f(x)$ . It is easy to see that  $\mathbb{E}(\epsilon(x)) = 0$  and  $\text{Var}(\epsilon(x)) = f(x)$ .

Let us set some notations to be used throughout the paper. The Euclidean norm of a vector  $x = (x_1, \dots, x_d) \in \mathbf{R}^d$  is denoted by  $\|x\|_2 = \left(\sum_{i=1}^d x_i^2\right)^{\frac{1}{2}}$ . The supremum norm of  $x$  is denoted by  $\|x\|_\infty = \sup_{1 \leq i \leq d} |x_i|$ . The cardinality of a set  $\mathbf{A}$  is denoted  $\text{card } \mathbf{A}$ . For a positive integer  $N$  the uniform  $N \times N$  grid of pixels on the unit square is defined by

$$\mathbf{I} = \left\{ \frac{1}{N}, \frac{2}{N}, \dots, \frac{N-1}{N}, 1 \right\}^2. \quad (3)$$

Each element  $x$  of the grid  $\mathbf{I}$  will be called pixel. The number of pixels is  $n = N^2$ . For any pixel  $x_0 \in \mathbf{I}$  and a given  $h > 0$ , the square window of pixels

$$\mathbf{U}_{x_0, h} = \{x \in \mathbf{I} : \|x - x_0\|_\infty \leq h\} \quad (4)$$

will be called *search window* at  $x_0$ . We naturally take  $h$  as a multiple of  $\frac{1}{N}$  ( $h = \frac{k}{N}$  for some  $k \in \{1, 2, \dots, N\}$ ). The size of the square search window  $\mathbf{U}_{x_0, h}$  is the positive integer number

$$M = (2Nh + 1)^2 = \text{card } \mathbf{U}_{x_0, h}. \quad (5)$$

For any pixel  $x \in \mathbf{U}_{x_0, h}$  and a given  $\eta > 0$  a second square window of pixels  $\mathbf{U}_{x, \eta}$  will be called *patch* at  $x$ . Like  $h$ , the parameter  $\eta$  is also taken as a multiple of  $\frac{1}{N}$ . The size of the patch  $\mathbf{U}_{x, \eta}$  is the positive integer

$$m = (2N\eta + 1)^2 = \text{card } \mathbf{U}_{x, \eta}. \quad (6)$$

## 2.2 The Non-Local Means algorithm

The Non-Local Means algorithm (2005 [8]) can be described as follows. For any  $x \in \mathbf{I}$ ,

$$\tilde{f} = \sum_{x \in \mathbf{I}} w(x)Y(x), \quad (7)$$

where the weights  $w(x)$  are given by

$$w(x) = e^{-\tilde{\rho}_{x_0}^2(x)/H^2} \Big/ \sum_{x' \in \mathbf{I}} e^{-\tilde{\rho}_{x_0}^2(x')/H^2}, \quad (8)$$

with

$$\tilde{\rho}_{x_0}^2 = \sum_{y \in \mathbf{U}_{x_0, \eta}} \frac{\kappa(y) |Y(y) - Y(T_x y)|^2}{\sum_{y' \in \mathbf{U}_{x_0, \eta}} \kappa(y')}.$$

Here  $H$  is a bandwidth parameter,  $\mathbf{U}_{x_0, \eta}$  is given by (4),  $\kappa(y) > 0$  are some fixed kernel, and  $T_x$  is the translation mapping:

$$T_x : x_0 + y \rightarrow x + y \quad (9)$$

In practice the bandwidth parameter  $H$  is often taken as a linear function of  $\sigma$  (see [8]).

### 2.3 Oracle estimator

In order to adapt the Non-Local Means algorithm to the Poisson noise, we introduce an "Oracle" estimator (for details on this concept see Donoho and Johnstone (1994 [11])). Denote

$$f_h^* = \sum_{x \in \mathbf{U}_{x_0, h}} w_h^* Y(x), \quad (10)$$

where

$$w_h^*(x) = e^{-\frac{\rho_{f, x_0}^2(x)}{H^2(x_0)}} \Big/ \sum_{x' \in \mathbf{U}_{x_0, h}} e^{-\frac{\rho_{f, x_0}^2(x')}{H^2(x_0)}} \quad (11)$$

with

$$\rho_{f, x_0}(x) \equiv |f(x) - f(x_0)|, \quad (12)$$

$H(x)$  is a control function subject to

$$\gamma = \inf\{H(x) : x \in \mathbf{I}\} > 0. \quad (13)$$

It is obvious that

$$\sum_{x \in \mathbf{U}_{x_0, h}} w_h^*(x) = 1 \quad \text{and} \quad w_h^*(x) \geq 0. \quad (14)$$

Note that the function  $\rho_{f, x_0}(x) \geq 0$  characterizes the similarity of the image brightness at the pixel  $x$  with respect to the pixel  $x_0$ , therefore we shall call

$\rho_{f,x_0}$  similarity function. The usual bias-variance decomposition (cf. e.g. [12, 30, 37]) of the Mean Squared Error (MSE)

$$\begin{aligned} & \mathbb{E} (f(x_0) - f_h^*(x_0))^2 \\ &= \left( \sum_{x \in \mathbf{U}_{x_0, h}} w_h^*(x) (f(x) - f(x_0)) \right)^2 + \sum_{x \in \mathbf{U}_{x_0, h}} w_h^*(x)^2 f(x) \\ &\leq \left( \sum_{x \in \mathbf{U}_{x_0, h}} w_h^*(x) |f(x) - f(x_0)| \right)^2 + \sum_{x \in \mathbf{U}_{x_0, h}} w_h^*(x)^2 f(x). \end{aligned} \quad (15)$$

The inequality (15) combining with (12) implies the following upper bound

$$\mathbb{E} (f(x_0) - f_h^*(x_0))^2 \leq g(w_h^*(x)), \quad (16)$$

where

$$g(w) = \left( \sum_{x \in \mathbf{U}_{x_0, h}} w(x) \rho_{f,x_0}(x) \right)^2 + \sum_{x \in \mathbf{U}_{x_0, h}} w(x)^2 f(x). \quad (17)$$

We shall define a family of estimates by minimizing the function  $g(w_h)$  by changing the width of the search window. With a Poisson noise in low-light conditions, the upper bound of signal function is small, so we let  $\Gamma = \sup\{f(x) : x \in \mathbf{I}\}$ . According to the similarity phenomenon existing very often in natural images, we suppose that the function  $f$  satisfies the local Hölder condition

$$|f(x) - f(y)| \leq L \|x - y\|_\infty^\beta, \quad \forall x, y \in \mathbf{U}_{x_0, h+\eta}, \quad (18)$$

where  $\beta > 0$  and  $L > 0$  are constants,  $h > 0$ ,  $\eta > 0$  and  $x_0 \in \mathbf{I}$ . The following theorem gives the rate of convergence of the "Oracle" estimator and the proper width  $h$  of the search window.

**Theorem 1** *Assume that  $h = \left(\frac{\Gamma}{4\beta L^2}\right)^{\frac{1}{2\beta+2}} n^{-\frac{1}{2\beta+2}}$  and  $\gamma > \sqrt{2}Lh^\beta$ . Suppose that the function  $f$  satisfies the local Hölder condition (18) and  $f_h^*(x_0)$  be given by (10). Then*

$$\mathbb{E} (f_h^*(x_0) - f(x_0))^2 \leq c_0 n^{-\frac{2\beta}{2\beta+2}}, \quad (19)$$

where

$$c_0 = \frac{2^{\frac{2\beta+6}{2\beta+2}} \Gamma^{\frac{2\beta}{2\beta+2}} L^{\frac{4}{2\beta+2}}}{\beta^{\frac{2\beta}{2\beta+2}}}. \quad (20)$$

For the proof of this theorem see Section 6.1.

This theorem shows that at least from the practical point of view, it is justified to optimize the upper bound  $g(w)$  instead of optimizing the risk  $\mathbb{E} (f_h^*(x_0) - f(x_0))^2$  itself. The theorem also justifies that we can choose a small search window in place of the whole observed image to estimate a point, without loss of visual quality. That is why we only consider small search windows for the simulations of our algorithm.

### 3 Non-Local Means Poisson Filter

#### 3.1 Construction of Non-Local Means Poisson Filter

With the theory of "Oracle" estimator, we construct the Non-Local Means Poisson Filter. Let  $h > 0$  and  $\eta > 0$  be fixed numbers. Since  $|f(x) - f(x_0)|^2 = \mathbb{E}|Y(x) - Y(x_0)|^2 - (f(x_0) + f(x))$ , an obvious estimator of  $\mathbb{E}|Y(x) - Y(x_0)|^2$  is given by

$$\frac{1}{M} \sum_{y \in \mathbf{U}_{x_0, \eta}} |Y(y) - Y(T_x y)|^2,$$

where  $T_x$  is given by (9), and  $(f(x_0) + f(x))$  is estimated by  $2\bar{f}(x_0)$ , where

$$\bar{f}(x_0) = \frac{1}{M} \sum_{x \in \mathbf{U}_{x_0, h}} f(x).$$

Define an estimated similarity function  $\hat{\rho}_{x_0}$  by

$$\hat{\rho}_{x_0}^2(x) = \left( \frac{1}{M} \sum_{y \in \mathbf{U}_{x_0, \eta}} |Y(y) - Y(T_x y)|^2 - 2\bar{f}(x_0) \right)^+. \quad (21)$$

The following theorem implies that it is reasonable to let  $\hat{\rho}_{x_0}(x)$  be the estimator of  $\rho_{f, x_0}(x)$ .

**Theorem 2** Assume that  $h = \left(\frac{\Gamma}{4\beta L^2}\right)^{\frac{1}{2\beta+2}} n^{-\frac{1}{2\beta+2}}$  and  $\eta = c_1 n^{-\alpha}$  ( $\frac{(1-\beta)^+}{2\beta+2} < \alpha < \frac{1}{2}$ ). Suppose that the function  $f$  satisfies the local Hölder condition (18) and  $\hat{\rho}_{x_0}^2(x)$  is given by (21). Then there is a constant  $c_2$  such that

$$\mathbb{P} \left\{ \max_{x \in \mathbf{U}_{x_0, h}} |\hat{\rho}_{x_0}^2(x) - \rho_{f, x_0}^2(x)| \geq c_2 n^{\alpha - \frac{1}{2}} \sqrt{\ln n} \right\} \leq O(n^{-1}). \quad (22)$$

For the proof of this theorem see Section 6.2.

As a result, it is natural to define an adaptive estimator  $\hat{f}_h$  by

$$\hat{f}_h(x_0) = \sum_{x \in \mathbf{U}_{x_0, h}} \hat{w}_h(x) Y(x), \quad (23)$$

where

$$\hat{w}_h = e^{-\frac{\hat{\rho}_{x_0}^2(x)}{H^2}} / \sum_{x' \in \mathbf{U}_{x_0, h}} e^{-\frac{\hat{\rho}_{x_0}^2(x')}{H^2}}. \quad (24)$$

and  $\mathbf{U}_{x_0, h}$  given by (4).

### 3.2 Convergence theorem of Non-Local Means Poisson Filter

Now, we turn to the study of the convergence of the Non-Local Means Poisson Filter. Due to the difficulty in dealing with the dependence of the weights we shall consider a slightly modified version of the proposed algorithm: we divide the set of pixels into two independent parts, so that the weights are constructed from the one part, and the estimation of the target function is a weighted mean along the other part. More precisely, we split the set of pixels into two parts  $\mathbf{I} = \mathbf{I}'_{x_0} \cup \mathbf{I}''_{x_0}$  for any  $x_0 \in \mathbf{I}$  where

$$\mathbf{I}'_{x_0} = \left\{ x_0 + \left( \frac{i}{N}, \frac{j}{N} \right) \in \mathbf{I} : i + j \text{ is even} \right\},$$

and  $\mathbf{I}''_{x_0} = \mathbf{I} \setminus \mathbf{I}'_{x_0}$ .

Define an estimated similarity function  $\hat{\rho}_{x_0}$  by

$$\hat{\rho}'_{x_0}(x) = \left( \frac{1}{\text{card}\mathbf{U}'_{x_0,\eta}} \sum_{y \in \mathbf{U}'_{x_0,\eta}} |Y(y) - Y(Txy)|^2 - 2\bar{f}'(x_0) \right)^+, \quad x \in \mathbf{U}'_{x_0,h} \quad (25)$$

where

$$\bar{f}'(x) = \frac{1}{\text{card}\mathbf{U}''_{x_0,h}} \sum_{y \in \mathbf{U}''_{x_0,h}} Y(y), \quad (26)$$

and  $\mathbf{U}'_{x_0,\eta} = \mathbf{U}_{x_0,\eta} \cap \mathbf{I}'_{x_0}$  with  $\mathbf{U}_{x_0,h}$  given by (4). The adaptive estimator  $\hat{f}'_h$  is denoted by

$$\hat{f}'_h(x_0) = \sum_{x \in \mathbf{U}'_{x_0,h}} \hat{w}'_h(x) Y(x), \quad (27)$$

where  $\mathbf{U}'_{x_0,h} = \mathbf{U}_{x_0,h} \cap \mathbf{I}'_{x_0}$  and

$$\hat{w}'_h = e^{-\frac{\hat{\rho}'_{x_0}(x)}{H^2(x_0)}} / \sum_{x' \in \mathbf{U}'_{x_0,h}} e^{-\frac{\hat{\rho}'_{x_0}(x')}{H^2(x_0)}}. \quad (28)$$

In the next theorem we prove that the Mean Squared Error of the estimator  $\hat{f}'_h(x_0)$  converges at the rate  $n^{-\frac{2\beta}{2\beta+2}}$  which is the usual optimal rate of convergence for a given Hölder smoothness  $\beta > 0$  (see e.g. Fan and Gijbels (1996 [13])).

**Theorem 3** Let  $\eta = c_3 n^{-\alpha}$ ,  $h = \left( \frac{\Gamma}{4\beta L^2} \right)^{\frac{1}{2\beta+2}} n^{-\frac{1}{2\beta+2}}$ ,  $H(x_0) > 4c_2 n^{\alpha-\frac{1}{2}} \sqrt{\ln n}$  and  $\gamma > \max\{\sqrt{2}Lh^\beta, 4c_2 n^{\alpha-\frac{1}{2}} \sqrt{\ln n}\}$ . Suppose that the function  $f$  satisfies the Hölder condition (18) and  $\hat{f}'_h(x_0)$  is given by (25). Then

$$\mathbb{E} \left( \hat{f}'_h(x_0) - f(x_0) \right)^2 \leq c_4 n^{-\frac{2\beta}{2\beta+2}}, \quad (29)$$



where

$$c_4 = 8 \left( \frac{2^{\frac{2\beta+6}{2\beta+2}} \Gamma^{\frac{2\beta}{2\beta+2}} L^{\frac{4}{2\beta+2}}}{\beta^{\frac{2\beta}{2\beta+2}}} \right)^2.$$

For the proof of this theorem see Section 6.2.

## 4 Simulation results

### 4.1 Computational algorithm

Throughout the simulations, we use the following algorithm to compute the Non-Local Means Poisson estimator  $\hat{f}_h(x_0)$ . The input values of the algorithm are  $Y(x)$ ,  $x \in \mathbf{I}$  (the image), and two numbers  $m$  and  $M$  are given by (6) and (5) respectively. In order to improve the results, we introduce a smoothed version of the estimated similarity distance

$$\hat{\rho}_{\kappa, x_0}^2(x) = \left( \sum_{y \in \mathbf{U}_{x_0, \eta}} \frac{\kappa(y) |Y(y) - Y(T_x y)|^2 - 2\bar{f}(x_0)}{\sum_{y' \in \mathbf{U}_{x_0, \eta}} \kappa(y')} \right)^+. \quad (30)$$

As smoothing kernels  $\kappa$  we use the Gaussian kernel

$$\kappa_g(y, h_g) = \exp\left(-\frac{N^2 \|y - x_0\|_2^2}{2h_g}\right), \quad (31)$$

where  $h_g$  is a constant, and the following kernel: for  $y \in \mathbf{U}_{x_0, \eta}$ ,

$$\kappa_0(y) = \sum_{k=\max(1, j)}^{N\eta} \frac{1}{(2k+1)^2}, \quad (32)$$

if  $\|y - x_0\|_\infty = \frac{j}{N}$  for some  $j \in \{0, 1, \dots, N\eta\}$ . We shall also use the rectangular kernel

$$\kappa_r(y) = \begin{cases} \frac{1}{\text{card}\mathbf{U}_{x_0, \eta}}, & y \in \mathbf{U}_{x_0, \eta}, \\ 0, & \text{otherwise.} \end{cases} \quad (33)$$

For the simulation we use the kernel  $\kappa_0(y)$  defined by (32). We have seen experimentally that when we take the filtering function  $H^2(x_0)$  as  $\mu \cdot \sqrt{\bar{f}(x_0)}$ , where  $\mu$  is a constant depending on the character of the image, to obtain a denoising of high visual quality. We mention that throughout the paper we symmetrize images near the boundary.

---

### Algorithm Non-Local Means Poisson Filter (NLMPF)

---

Let  $\{M, m, h_g\}$  be the parameters.  
Repeat for each  $x_0 \in \mathbf{I}$

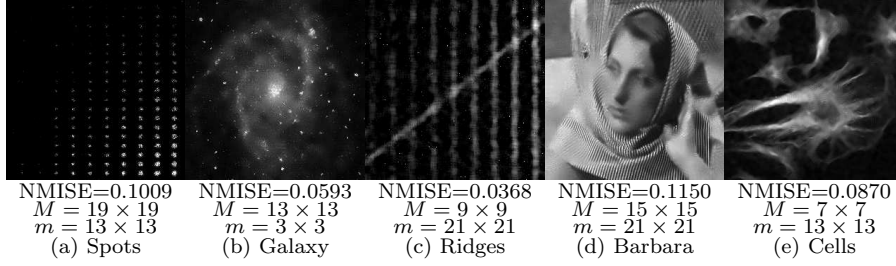


**Fig. 1** These images restored by the first step of our algorithm.

- compute

**Step 1**

$$\hat{w}(x) = \exp(-\hat{\rho}_{\kappa, x_0}^2(x)/H^2(x_0))$$

$$\hat{f}_1(x_0) = \sum_{x \in \mathbf{U}_{x_0, h}} \hat{w}(x) Y(x) / \sum_{x \in \mathbf{U}_{x_0, h}} w(x)$$

**Step 2**

$$\text{If } \frac{1}{(2d+1)^d} \sum_{\|x-x_0\| \leq d/N} \hat{f}_1(x) < \delta$$

$$\text{compute } \hat{f}(x_0) = \sum_{\|x-x_0\| \leq d/N} \kappa_g(x, h_g) \hat{f}_1(x) / \sum_{\|x-x_0\| \leq d/N} \kappa_g(x, h_g)$$

$$\text{else } \hat{f}(x_0) = \hat{f}_1(x_0).$$

---

*Note:* we take  $\delta = 15$ .

#### 4.2 Numerical performance of the Non-Local Means Poisson Filter

By simulations we found that the images with brightness between 0 and 255 (like Barbara) are well denoised by the first step, but for the low count level images (with brightness less than  $\mu$ ), the restored images by NLMPF are not smooth enough (see Figure 1). This explains why for the low count level images, we smooth the restored images by step 2.

Our experiments are done in the same way as in [39] and [28] to produce comparable results; we also use the same set of test images (all of  $256 \times 256$  in size): Spots [0.08, 4.99], Galaxy [0, 5], Ridges [0.05, 0.85], Barbara [0.93, 15.73], and Cells [0.53, 16.93]. The authors of [39] and [28] kindly provided us with their programs and the test images. A matlab implementation of the algorithms derived in this paper is available online<sup>1</sup>. This unoptimized implementation processes the set of  $256 \times 256$  test images 145 seconds with a search window of size  $15 \times 15$  and patches of size  $21 \times 21$ , 52 seconds with a search window of size  $9 \times 9$  and patches of size  $21 \times 21$ . The computational time is of about 10s per iteration on a  $256 \times 256$  image and Matlab on an Intel Pentium Dual CPU T3200 32-bit @ 2.00GHz CPU 3.00GHz.

<sup>1</sup> <http://www.pami.sjtu.edu.cn/people/jinqy/>

**Table 1** A comparison of the denoising performance (NMISE) of several denoising algorithms.

Algorithm	Our algorithm	OWPNF	Poisson NLM	EUI+ BM3D	MS-VST +7/9	MS-VST +B3
Spots[0.08, 4.99]	0.0260	<b>0.0259</b>	0.0790	0.0358	0.0602	0.0810
Galaxy[0, 5]	<b>0.0284</b>	0.0285	0.0346	0.0297	0.0357	0.0338
Ridges[0.05, 0.85]	0.0140	0.0162	0.0154	<b>0.0121</b>	0.0193	0.0416
Barbara[0.93, 15.73]	0.1150	0.1061	0.1207	<b>0.0863</b>	0.2391	0.3777
Cells[0.53, 16.93]	0.0785	0.0794	0.0816	<b>0.0643</b>	0.0909	0.1487

**Table 2** A comparison of the denoising performance (PSNR, DB) of several denoising algorithms.

Algorithm	Our algorithm	OWPNF	Poisson NLM	EUI+ BM3D	MS-VST +7/9	MS-VST +B3
Spots[0.08, 4.99]	31.45	31.31	31.12	<b>31.95</b>	31.64	30.35
Galaxy[0, 5]	<b>28.09</b>	27.80	27.77	28.04	27.57	27.94
Ridges[0.05, 0.85]	24.69	23.90	24.94	<b>25.89</b>	24.49	24.03
Barbara[0.93, 15.73]	24.71	24.60	24.72	<b>25.92</b>	21.81	20.22
Cells[0.53, 16.93]	29.08	29.91	29.40	<b>30.18</b>	28.87	26.69

Table 1 shows the NMISE values of images reconstructed by NLMPF, OWPNF [19], Poisson NLM [10], EUI+BM3D [29], MS-VST+7/9 [39] and MS-VST+B3 [39]. Our algorithm reach the best in the case of Galaxy[0, 5], while OWPNF reach the best in the case of Spots[0.08, 4.99]; for Ridges[0.05, 0.85], Barbara[0.93, 15.73], and Cells[0.53, 16.93], the method EUI+BM3D gives the best results, but our method is also very competitive. Table 2 shows the PSNR values of images reconstructed. Our algorithm also reach the best in the case of Galaxy[0, 5]. The method EUI+BM3D have the highest PSNR value. However, the most important evaluation criteria is the visual quality of restored image. Figures 2- 6 illustrate the visual quality of these denoised images. It is obvious that The visual quality of the outputs of our method have high visual quality and many details Remained. For example, in the case of restored images of Spots (cf. Figures 2), our algorithm and OWPNF remain most spots. We can see clearly 7 spots at the third column (from left) in Figures 2 (c), while EUI+BM3D just remains 4 spots, Poisson NLM Makes several spots sticking together, the images restored by MS-VST + 7/9 and MS-VST + B3 are not smooth enough. In the case of Galaxy (cf. Figures 3), visually, our algorithm best preserves the fine textures. In the other case, our method also lead to good result visually.

## 5 Conclusion

In this paper, we have present a new image denoising algorithm to deal with the Poisson noise model, which is based on the idea of Non-Local Mean. The "Oracle" estimator is obtained by minimized a very tight upper bound of the Mean Square Error with changing the size of search window. It help to establish a theorem to show that the Non-Local Means Filter can effectively deal with Poisson noise with some modification. As a result, we successfully construct the new algorithm called Non-Local Means Poisson Filter and demonstrate in statistic theory that the filter converges at the usual optimal rate. The filter is as simple as the classic Non-Local Means and the simulation results show that our filter is very competitive. The idea of how to construct an algorithm for Poisson noise model is creative. With our idea, many algorithms to Remove Gaussian Noise could deal with the Poisson noise with some modification.

## 6 Appendix: Proofs of the main results

### 6.1 Proof of Theorem 1

Denoting for brevity

$$I_1 = \left( \sum_{x \in \mathbf{U}_{x_0, h}} w_h^*(x) \rho_{f, x_0}(x) \right)^2 = \left( \frac{\sum_{\|x-x_0\|_\infty \leq h} e^{-\frac{\rho_{f, x_0}^2(x)}{H^2(x_0)}} \rho_{f, x_0}(x)}{\sum_{\|x-x_0\|_\infty \leq h} e^{-\frac{\rho_{f, x_0}^2(x)}{H^2(x_0)}}} \right)^2, \quad (34)$$

and

$$I_2 = f(x_0) \sum_{x \in \mathbf{U}_{x_0, h}} (w_h^*(x))^2 = \frac{f(x_0) \sum_{\|x-x_0\|_\infty \leq h} e^{-2\frac{\rho_{f, x_0}^2(x)}{H^2(x_0)}}}{\left( \sum_{\|x-x_0\|_\infty \leq h} e^{-\frac{\rho_{f, x_0}^2(x)}{H^2(x_0)}} \right)^2}, \quad (35)$$

then we have

$$g(w_h^*) = I_1 + I_2. \quad (36)$$

The conditions (13) and  $\gamma > \sqrt{2}Lh^\beta$  imply that for  $x \in U_{x_0, h}$ , we have

$$\frac{L^2 \|x - x_0\|_\infty^{2\beta}}{H^2(x)} \leq \frac{L^2 h^{2\beta}}{\gamma^2} \leq \frac{1}{2}. \quad (37)$$

Noting that  $e^{-\frac{t^2}{H^2(x_0)}}$ ,  $t \in [0, \gamma/\sqrt{2}]$  is decreasing, and using one term Taylor expansion, the inequality (37) implies that

$$\begin{aligned} \sum_{\|x-x_0\|_\infty \leq h} e^{-\frac{\rho_{f,x_0}^2(x)}{H^2(x_0)}} &\geq \sum_{\|x-x_0\|_\infty \leq h} e^{-\frac{L^2\|x-x_0\|_\infty^{2\beta}}{H^2(x_0)}} \geq \sum_{\|x-x_0\|_\infty \leq h} \left(1 - \frac{L^2\|x-x_0\|_\infty^{2\beta}}{H^2(x_0)}\right) \\ &\geq 2h^2n. \end{aligned} \quad (38)$$

Considering that  $te^{-\frac{t^2}{H^2(x_0)}}$ ,  $t \in [0, \gamma/\sqrt{2}]$  is increasing function,

$$\begin{aligned} \sum_{\|x-x_0\|_\infty \leq h} e^{-\frac{\rho_{f,x_0}^2(x)}{H^2(x_0)}} \rho_{f,x_0}(x) &\leq \sum_{\|x-x_0\|_\infty \leq h} L\|x-x_0\|_\infty^\beta e^{-\frac{L^2\|x-x_0\|_\infty^{2\beta}}{H^2(x_0)}} \\ &\leq \sum_{\|x-x_0\|_\infty \leq h} L\|x-x_0\|_\infty^\beta \leq 4Lh^{\beta+2}n. \end{aligned} \quad (39)$$

The above three inequalities (34), (38) and (39) imply that

$$I_1 \leq 4L^2h^{2\beta}. \quad (40)$$

Taking into account the inequality

$$\sum_{\|x-x_0\|_\infty \leq h} e^{-2\frac{\rho_{f,x_0}^2(x)}{H^2(x_0)}} \leq \sum_{\|x-x_0\|_\infty \leq h} 1 = 4h^2n,$$

(35) and (38), it is easily seen that

$$I_2 \leq \frac{\Gamma}{h^2n}. \quad (41)$$

Combining (36), (40), and (41), we give

$$g(w_h^*) \leq 4L^2h^{2\beta} + \frac{\Gamma}{h^2n}. \quad (42)$$

Let  $h$  minimize the latter term of the above inequality (42). Then

$$8\beta L^2h^{2\beta-1} - \frac{2\Gamma}{h^3n} = 0$$

from which we infer that

$$h = \left(\frac{\Gamma}{4\beta L^2}\right)^{\frac{1}{2\beta+2}} n^{-\frac{1}{2\beta+2}}. \quad (43)$$

Substituting (43) to (42) leads to

$$g(w_h^*) \leq \frac{2^{\frac{2\beta+6}{2\beta+2}} \Gamma^{\frac{2\beta}{2\beta+2}} L^{\frac{4}{2\beta+2}}}{\beta^{\frac{2\beta}{2\beta+2}}} n^{-\frac{2\beta}{2\beta+2}}.$$

Therefore (16) implies (19).

## 6.2 Proof of Theorem 2

We shall use following lemma to finish the Proof of Theorem 2. The lemma can be deduced from the results in Borovkov [6], see also Merlevede, Peligrad and Rio [31]

**Lemma 1** *If, for some  $\delta > 0, \gamma \in (0, 1)$  and  $K > 1$  we have*

$$\sup \mathbb{E} \exp(\delta |X_i|^\gamma) \leq K, \quad i = 1, \dots, n,$$

*then there are two positive constants  $c_1$  and  $c_2$  depending only on  $\delta, \gamma$  and  $K$  such that, for any  $t > 0$ ,*

$$\mathbb{P} \left( \sum_{i=1}^n X_i \geq t \right) \leq \exp(-c_1 t^2/n) + n \exp(-c_2 t^\gamma).$$

**Proof of Theorem 2.** Recall that  $M$  and  $m$  is given by (5) and (6) respectively. Consider that

$$|\widehat{\rho}_{x_0}^2(x) - \rho_{f, x_0}^2(x)| \leq \left| \frac{1}{m} S(x) + \frac{1}{m} R(x) \right|, \quad (44)$$

where

$$S(x) = \sum_{y \in \mathbf{U}_{x_0, \eta}} Z(y),$$

$$Z(y) = (Y(y) - Y(T_x y))^2 - (f(y) - f(T_x y))^2 - f(y) - f(T_x y), \quad (45)$$

and

$$R(x) = \sum_{y \in \mathbf{U}_{x_0, \eta}} ((f(y) - f(T_x y))^2 + f(y) + f(T_x y)) - (f(x_0) - f(x))^2 - 2\bar{f}(x_0).$$

Since  $Y(x)$  has the Poisson distribution, with mean  $f(x)$  and variance  $f(x)$ ,

$$\mathbb{E} \left( e^{Y(x)} \right) = \sum_{k=0}^{+\infty} e^k \frac{f^k(x) e^{-f(x)}}{k!} = e f(x) e^{(e-1)f(x)} \leq e \Gamma e^{(e-1)\Gamma}. \quad (46)$$

From the inequality (46), we easily deduce

$$\sup \mathbb{E} \left( e^{|Z(y)|^{1/2}} \right) \leq \sup \mathbb{E} \left( e^{Y(y) + Y(T_x y) + 2\Gamma + 2\sqrt{\Gamma}} \right) \leq (e\Gamma)^2 e^{2e\Gamma + 2\sqrt{\Gamma}} \quad (47)$$

By Lemma 1, we see that there are two positive constants  $c_5$  and  $c_6$  such that for any  $z > 0$ ,

$$\mathbb{P} \left( \frac{1}{m} |S(x)| \geq \frac{z}{\sqrt{m}} \right) \leq \exp(-c_5 z^2) + m \exp(-c_6 (\sqrt{m} z)^{\frac{1}{2}}). \quad (48)$$

Considering  $m = (2N\eta + 1)^2$  and  $\eta = c_1 n^{-\alpha} \left( \frac{(1-\beta)^+}{2\beta+2} \right) < \alpha < \frac{1}{2}$ , we have  $m = c_1' n^{1-2\alpha} (1 + o(1))$ . Therefore, substituting  $z = \sqrt{\frac{1}{c_5} \ln n^2}$  into the inequality (48), we see that for  $n$  large enough,

$$\mathbb{P} \left( \frac{1}{m} |S(x)| \geq \frac{\sqrt{\frac{1}{c_5} \ln n^2}}{\sqrt{m}} \right) \leq 2 \exp(-\ln n^2) = \frac{2}{n^2}.$$

From this inequality we easily deduce that

$$\mathbb{P} \left( \max_{x \in \mathbf{U}_{x_0, h}} \frac{1}{m} |S(x)| \geq \frac{\sqrt{\frac{1}{c_5} \ln n^2}}{\sqrt{m}} \right) \leq \sum_{x \in \mathbf{U}_{x_0, h}} \mathbb{P} \left( \frac{1}{m} |S(x)| \geq \frac{\sqrt{\frac{1}{c_5} \ln n^2}}{\sqrt{m}} \right) \leq \frac{2}{n}.$$

We arrive at

$$\mathbb{P}(\mathbf{B}) \leq c_7 n^{-1}, \quad (49)$$

where  $\mathbf{B} = \{\max_{x \in \mathbf{U}_{x_0, h}} \frac{1}{m} |S(x)| < c_8 n^{\alpha - \frac{1}{2}} \sqrt{\ln n}\}$  and  $c_8$  is a constant depending only on  $\beta$  and  $L$ . It is easy to see that

$$R(x) = O\left(n^{\alpha - \frac{1}{2}}\right). \quad (50)$$

In the set  $\mathbf{B}$ , the inequality (50) implies that

$$\max_{x \in \mathbf{U}_{x_0, h}} |\hat{\rho}_{x_0}^2(x) - \rho_{f, x_0}^2(x)| \leq c_8 n^{-\frac{\beta}{2\beta+2}} \sqrt{\ln n} + O\left(n^{\alpha - \frac{1}{2}}\right) = O\left(n^{-\frac{\beta}{2\beta+2}} \sqrt{\ln n}\right). \quad (51)$$

Combining (49) and (51), we obtain (22).

### 6.3 Proof of Theorem 3

Taking into account (25), (27), and the independence of  $\epsilon(x)$ , we have

$$\mathbb{E}\{|\hat{f}_h'(x_0) - f(x_0)|^2 | Y(x), x \in \mathbf{I}_{x_0}''\} \leq g'(\hat{w}_h), \quad (52)$$

where

$$g'(w) = \left( \sum_{x \in \mathbf{U}'_{x_0, h}} w(x) \rho_{f, x_0}(x) \right)^2 + \bar{f}'(x_0) \sum_{x \in \mathbf{I}'_{x_0}} w^2(x).$$

By the proof of Theorem 1, we obtain

$$g'(w_h^*) \leq \frac{3}{2} \left( \frac{2^{\frac{2\beta+6}{2\beta+2}} \Gamma^{\frac{2\beta}{2\beta+2}} L^{\frac{4}{2\beta+2}}}{\beta^{\frac{2\beta}{2\beta+2}}} n^{-\frac{2\beta}{2\beta+2}} \right). \quad (53)$$

By Theorem 2 and its proof, for  $\hat{\rho}_{x_0}'$  is defined by (25), there is a constant  $c_2$  such that

$$\mathbb{P} \left\{ \max_{x \in \mathbf{U}'_{x_0, h}} \left| \hat{\rho}_{x_0}'^2(x) - \rho_{f, x_0}^2(x) \right| \geq c_2 n^{\alpha - \frac{1}{2}} \sqrt{\ln n} \right\} = O(n^{-1}). \quad (54)$$

Let  $\mathbf{B} = \left\{ \max_{x \in \mathbf{U}'_{x_0, h}} \left| \hat{\rho}_{x_0}^{\prime 2}(x) - \rho_{f, x_0}^2(x) \right| \leq c_2 n^{\alpha - \frac{1}{2}} \ln n \right\}$ . On the set  $\mathbf{B}$ , we have  $\rho_{f, x_0}^2(x) - c_2 n^{\alpha - \frac{1}{2}} \sqrt{\ln n} < \hat{\rho}_{x_0}^{\prime 2}(x) < \rho_{f, x_0}^2(x) + c_2 n^{\alpha - \frac{1}{2}} \sqrt{\ln n}$ , from which we infer that

$$\begin{aligned} \hat{w}(x) &= \frac{e^{-\frac{\hat{\rho}_{x_0}^{\prime 2}(x)}{H^2(x_0)}}}{\sum_{x' \in \mathbf{U}'_{x_0, h}} e^{-\frac{\hat{\rho}_{x_0}^{\prime 2}(x')}{H^2(x_0)}}} \leq \frac{e^{-\frac{\rho_{f, x_0}^2(x) - c_2 n^{\alpha - \frac{1}{2}} \sqrt{\ln n}}{H^2(x_0)}}}{\sum_{x' \in \mathbf{U}'_{x_0, h}} e^{-\frac{\rho_{f, x_0}^2(x') + c_2 n^{\alpha - \frac{1}{2}} \sqrt{\ln n}}{H^2(x_0)}}} \\ &\leq \frac{e^{-\frac{\rho_{f, x_0}^2(x)}{H^2(x_0)}} \left( 1 + \frac{2c_2 n^{\alpha - \frac{1}{2}} \sqrt{\ln n}}{H^2(x_0)} \right)}{\sum_{x' \in \mathbf{U}'_{x_0, h}} e^{-\frac{\rho_{f, x_0}^2(x')}{H^2(x_0)}} \left( 1 - \frac{c_2 n^{\alpha - \frac{1}{2}} \sqrt{\ln n}}{H^2(x_0)} \right)} \\ &= \left( \frac{1 + \frac{2c_2 n^{\alpha - \frac{1}{2}} \sqrt{\ln n}}{H^2(x_0)}}{1 - \frac{c_2 n^{\alpha - \frac{1}{2}} \sqrt{\ln n}}{H^2(x_0)}} \right) \frac{e^{-\frac{\rho_{f, x_0}^2(x)}{H^2(x_0)}}}{\sum_{x' \in \mathbf{U}'_{x_0, h}} e^{-\frac{\rho_{f, x_0}^2(x')}{H^2(x_0)}}} \\ &= \left( \frac{1 + \frac{2c_2 n^{\alpha - \frac{1}{2}} \sqrt{\ln n}}{H^2(x_0)}}{1 - \frac{c_2 n^{\alpha - \frac{1}{2}} \sqrt{\ln n}}{H^2(x_0)}} \right) w_h^*(x). \end{aligned}$$

This implies that

$$g'(\hat{w}_h) \leq \left( \frac{1 + \frac{2c_2 n^{\alpha - \frac{1}{2}} \sqrt{\ln n}}{H^2(x_0)}}{1 - \frac{c_2 n^{\alpha - \frac{1}{2}} \sqrt{\ln n}}{H^2(x_0)}} \right)^2 g'(w_h^*).$$

The condition  $4c_2 n^{\alpha - \frac{1}{2}} \sqrt{\ln n} < \gamma \leq H^2(x_0)$  implies that

$$\left( \frac{1 + \frac{2c_2 n^{\alpha - \frac{1}{2}} \sqrt{\ln n}}{H^2(x_0)}}{1 - \frac{c_2 n^{\alpha - \frac{1}{2}} \sqrt{\ln n}}{H^2(x_0)}} \right)^2 \leq 2.$$

Consequently, (52) becomes

$$\mathbb{E} \left( |\hat{f}'_h(x_0) - f(x_0)|^2 | Y(x), x \in \mathbf{I}''_{x_0}, \mathbf{B} \right) \leq 2g'(w_h^*). \quad (55)$$

Since the function  $f$  satisfies the Hölder condition,

$$\mathbb{E} \left( |\hat{f}'_h(x_0) - f(x_0)|^2 | Y(x), x \in \mathbf{I}''_{x_0} \right) < g'(\hat{w}_h) \leq c_9, \quad (56)$$



for a constant  $c_9 > 0$  depending only on  $\beta$  and  $L$ . Combining (22), (55), and (56), we have

$$\begin{aligned} & \mathbb{E} \left( |\widehat{f}_h(x_0) - f(x_0)|^2 | Y(x), x \in \mathbf{I}''_{x_0} \right) \\ &= \mathbb{E} \left( |\widehat{f}'_h(x_0) - f(x_0)|^2 | Y(x), x \in \mathbf{I}''_{x_0}, \mathbf{B} \right) \mathbb{P}(\mathbf{B}) \\ & \quad + \mathbb{E} \left( |\widehat{f}'_h(x_0) - f(x_0)|^2 | Y(x), x \in \mathbf{I}''_{x_0}, \overline{\mathbf{B}} \right) \mathbb{P}(\overline{\mathbf{B}}) \\ & \leq 2g'(w_h^*) + O(n^{-1}) \end{aligned}$$

Now, the assertion of the theorem is obtained easily if we take into account (53).

## References

1. I. Abraham, R. Abraham, A. Desolneux, and S. Li-Thiao-Te. Significant edges in the case of non-stationary gaussian noise. *Pattern recognition*, 40(11):3277–3291, 2007.
2. M. Aharon, M. Elad, and A. Bruckstein. *rmk*-svd: An algorithm for designing overcomplete dictionaries for sparse representation. *IEEE Trans. Signal Process.*, 54(11):4311–4322, 2006.
3. F. Alter, Y. Matsushita, and X. Tang. An intensity similarity measure in low-light conditions. *Computer Vision–ECCV 2006*, pages 267–280, 2006.
4. F.J. Anscombe. The transformation of poisson, binomial and negative-binomial data. *Biometrika*, 35(3/4):246–254, 1948.
5. A. Beck and M. Teboulle. Fast gradient-based algorithms for constrained total variation image denoising and deblurring problems. *IEEE Trans. Image Process.*, 18(11):2419–2434, 2009.
6. A.A. Borovkov. Estimates for the distribution of sums and maxima of sums of random variables without the cramer condition. *Siberian Mathematical Journal*, 41(5):811–848, 2000.
7. J. Boulanger, J.B. Sibarita, C. Kervrann, and P. Bouthemy. Non-parametric regression for patch-based fluorescence microscopy image sequence denoising. In *in Proc. of IEEE Int. Symp. on Biomedical Imaging: From Nano to Macro, ISBI2008*, pages 748–751. IEEE, 2008.
8. A. Buades, B. Coll, and J.M. Morel. A review of image denoising algorithms, with a new one. *SIAM Journal on Multiscale Modeling and Simulation*, 4(2):490–530, 2005.
9. T. Buades, Y. Lou, JM Morel, and Z. Tang. A note on multi-image denoising. In *Int. workshop on Local and Non-Local Approximation in Image Processing*, pages 1–15, August 2009.
10. C.A. Deledalle, F. Tupin, and L. Denis. Poisson nl means: Unsupervised non local means for poisson noise. In *IEEE Int. Conf. on Image Process. (ICIP), 2010 17th*, pages 801–804. IEEE, 2010.
11. D.L. Donoho and J.M. Johnstone. Ideal spatial adaptation by wavelet shrinkage. *Biometrika*, 81(3):425, 1994.

12. J. Fan. Local linear regression smoothers and their minimax efficiencies. *The Annals of Statistics*, pages 196–216, 1993.
13. J.Q. Fan and I. Gijbels. Local polynomial modelling and its applications. In *Chapman & Hall, London*, 1996.
14. P. Fryzlewicz, V. Delouille, and G.P. Nason. Goes-8 x-ray sensor variance stabilization using the multiscale data-driven haar–fisz transform. *J. Roy. Statist. Soc. ser. C*, 56(1):99–116, 2007.
15. P. Fryzlewicz and G.P. Nason. A haar–fisz algorithm for poisson intensity estimation. *J. Comp. Graph. Stat.*, 13(3):621–638, 2004.
16. D.K. Hammond and E.P. Simoncelli. Image modeling and denoising with orientation-adapted gaussian scale mixtures. *IEEE Trans. Image Process.*, 17(11):2089–2101, 2008.
17. K. Hirakawa and T.W. Parks. Image denoising using total least squares. *IEEE Trans. Image Process.*, 15(9):2730–2742, 2006.
18. M. Jansen. Multiscale poisson data smoothing. *J. Roy. Statist. Soc. B*, 68(1):27–48, 2006.
19. Qiyu Jin, Ion Grama, and Quansheng Liu. A new poisson noise filter based on weights optimization. *arXiv preprint arXiv:1201.5968*, 2012.
20. Q.Y. Jin, I. Grama, and Q.S. Liu. Removing gaussian noise by optimization of weights in non-local means. <http://arxiv.org/abs/1109.5640>.
21. V. Katkovnik, A. Foi, K. Egiazarian, and J. Astola. From local kernel to nonlocal multiple-model image denoising. *Int. J. Comput. Vis.*, 86(1):1–32, 2010.
22. C. Kervrann and J. Boulanger. Optimal spatial adaptation for patch-based image denoising. *IEEE Trans. Image Process.*, 15(10):2866–2878, 2006.
23. E.D. Kolaczyk and R.D. Nowak. Multiscale generalised linear models for nonparametric function estimation. *Biometrika*, 92(1):119, 2005.
24. T. Le, R. Chartrand, and T. J. Asaki. A variational approach to reconstructing images corrupted by poisson noise. *Journal of Mathematical Imaging and Vision*, 27(3):257–263, 2007.
25. S. Lefkimiatis, P. Maragos, and G. Papandreou. Bayesian inference on multiscale models for poisson intensity estimation: Applications to photon-limited image denoising. *IEEE Trans. Image Process.*, 18(8):1724–1741, 2009.
26. F. Luisier, C. Vonesch, T. Blu, and M. Unser. Fast interscale wavelet denoising of poisson-corrupted images. *Signal Process.*, 90(2):415–427, 2010.
27. J. Mairal, G. Sapiro, and M. Elad. Learning multiscale sparse representations for image and video restoration. *SIAM Multiscale Modeling and Simulation*, 7(1):214–241, 2008.
28. M. Makitalo and A. Foi. On the inversion of the anscombe transformation in low-count poisson image denoising. In *Proc. Int. Workshop on Local and Non-Local Approx. in Image Process., LNLA 2009, Tuusula, Finland*, pages 26–32. IEEE, 2009.

29. M. Makitalo and A. Foi. Optimal inversion of the anscombe transformation in low-count poisson image denoising. *IEEE Trans. Image Process.*, 20(1):99–109, 2011.
30. J. Mandel. Use of the singular value decomposition in regression analysis. *The American Statistician*, 36(1):15–24, 1982.
31. F. Merlevède, M. Peligrad, and E. Rio. A bernstein type inequality and moderate deviations for weakly dependent sequences. *Probab. Theory Related Fields*, 2010.
32. I. Moon and B. Javidi. Three dimensional imaging and recognition using truncated photon counting model and parametric maximum likelihood estimator. *Optics express*, 17(18):15709–15715, 2009.
33. R.D. Nowak and E.D. Kolaczyk. A statistical multiscale framework for poisson inverse problems. *IEEE Trans. Info. Theory*, 46(5):1811–1825, 2000.
34. J. Polzehl and V. Spokoiny. Propagation-separation approach for local likelihood estimation. *Probab. Theory Rel.*, 135(3):335–362, 2006.
35. J. Portilla, V. Strela, M.J. Wainwright, and E.P. Simoncelli. Image denoising using scale mixtures of gaussians in the wavelet domain. *IEEE Trans. Image Process.*, 12(11):1338–1351, 2003.
36. S. Roth and M.J. Black. Fields of experts. *Int. J. Comput. Vision*, 82(2):205–229, 2009.
37. G. R. Terrell and D. W. Scott. Variable kernel density estimation. *The Annals of Statistics*, pages 1236–1265, 1992.
38. G.M.P. van Kempen, H.T.M. van der Voort, J.G.J. Bauman, and K.C. Strasters. Comparing maximum likelihood estimation and constrained tikhonov-miller restoration. *IEEE Engineering in Medicine and Biology Magazine*, 15(1):76–83, 1996.
39. B. Zhang, J.M. Fadili, and J.L. Starck. Wavelets, ridgelets, and curvelets for poisson noise removal. *IEEE Trans. Image Process.*, 17(7):1093–1108, 2008.

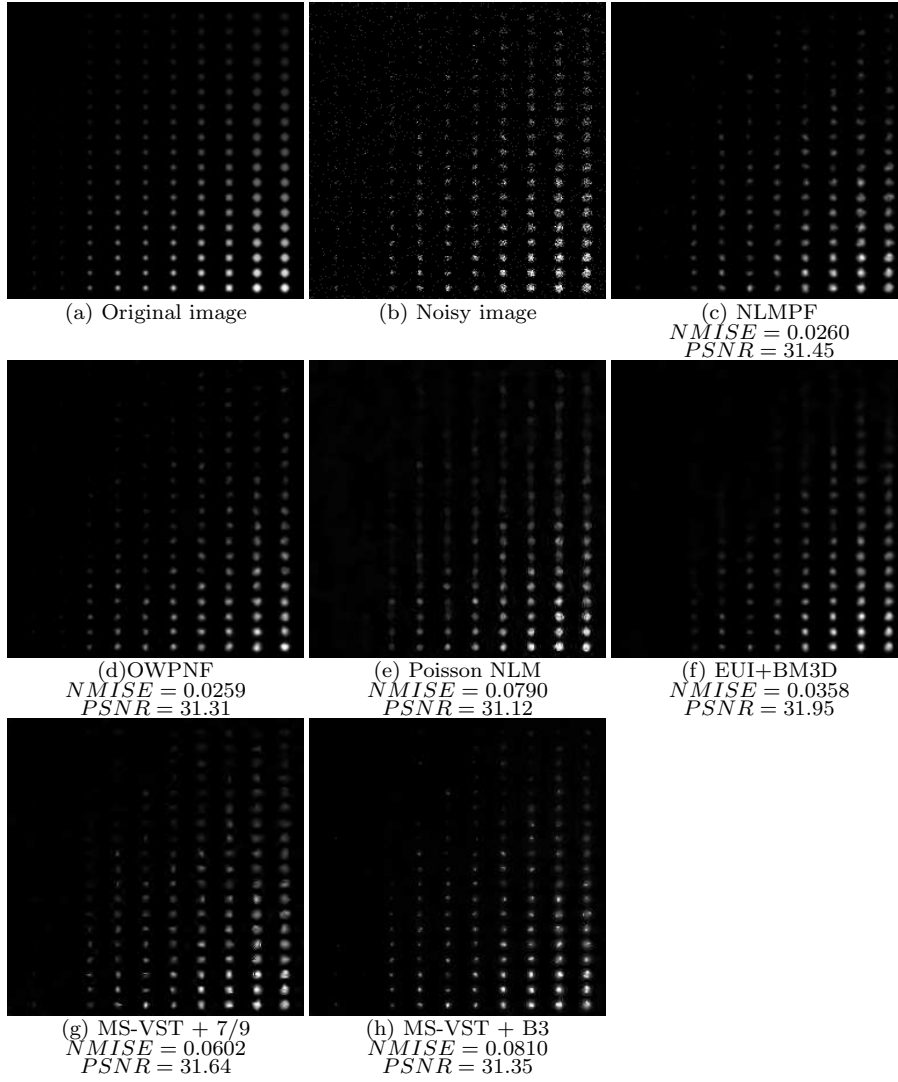


**Fig. 2** Denoising an image of simulated spots of different radii (image size:  $256 \times 256$ ). (a) simulated sources (amplitudes  $\in [0.08, 4.99]$ ; background = 0.03); (b) observed counts; (c) NLMPF ( $M = 19 \times 19$ ,  $m = 13 \times 13$ ,  $d = 3$ ,  $\sigma_H = 2.5$ ,  $\mu = 1$   $NMISE = 0.0260$ ); (d) Optimal Weights Filter ( $M = 19 \times 19$ ,  $m = 13 \times 13$ ,  $d = 2$  and  $H = 1$ ,  $NMISE = 0.0259$ ); (e) Poisson NLM ( $NMISE = 0.0790$ ); (f) Exact unbiased inverse + BM3D ( $NMISE = 0.0358$ ); (g) MS-VST + 7/9 biorthogonal wavelet ( $J = 5$ ,  $FPR = 0.01$ ,  $N_{max} = 5$  iterations,  $NMISE = 0.0602$ ); (h) MS-VST + B3 isotropic wavelet ( $J = 5$ ,  $FPR = 0.01$ ,  $N_{max} = 5$  iterations,  $NMISE = 0.0810$ ).

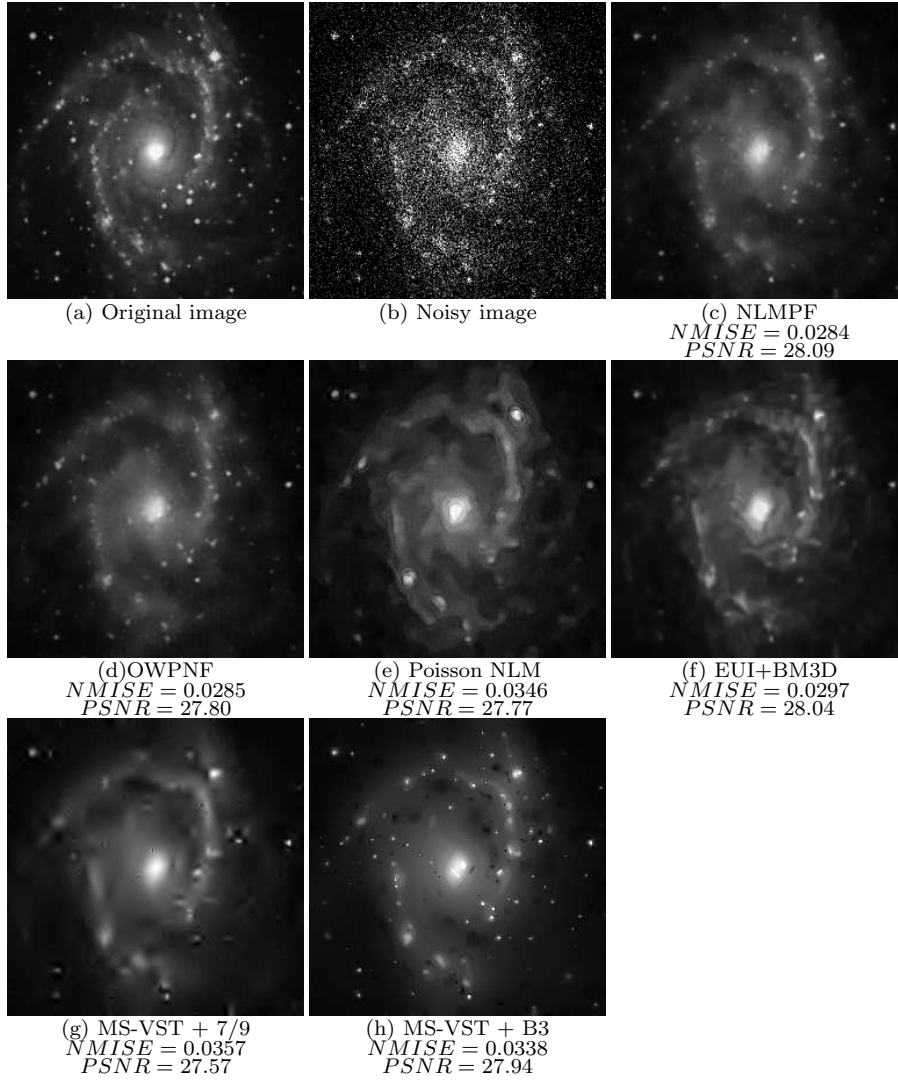


**Fig. 3** Denoising a galaxy image (image size:  $256 \times 256$ ). (a) galaxy image (intensity  $\in [0, 5]$ ); (b) observed counts; (c) NLMPF ( $M = 13 \times 13$ ,  $m = 3 \times 3$ ,  $d = 2$ ,  $\sigma_H = 1$ ,  $\mu = 0.6$   $NMISE = 0.0284$ ); (d) Optimal Weights Filter ( $M = 15 \times 15$ ,  $m = 5 \times 5$ ,  $d = 2$  and  $H = 1$ ,  $NMISE = 0.0285$ ); (e) Poisson NLM ( $NMISE = 0.0346$ ); (f) Exact unbiased inverse + BM3D ( $NMISE = 0.0297$ ); (g) MS-VST + 7/9 biorthogonal wavelet ( $J = 5$ ,  $FPR = 0.0001$ ,  $N_{max} = 5$  iterations,  $NMISE = 0.0357$ ); (h) MS-VST + B3 isotropic wavelet ( $J = 3$ ,  $FPR = 0.0001$ ,  $N_{max} = 10$  iterations,  $NMISE = 0.0338$ ).

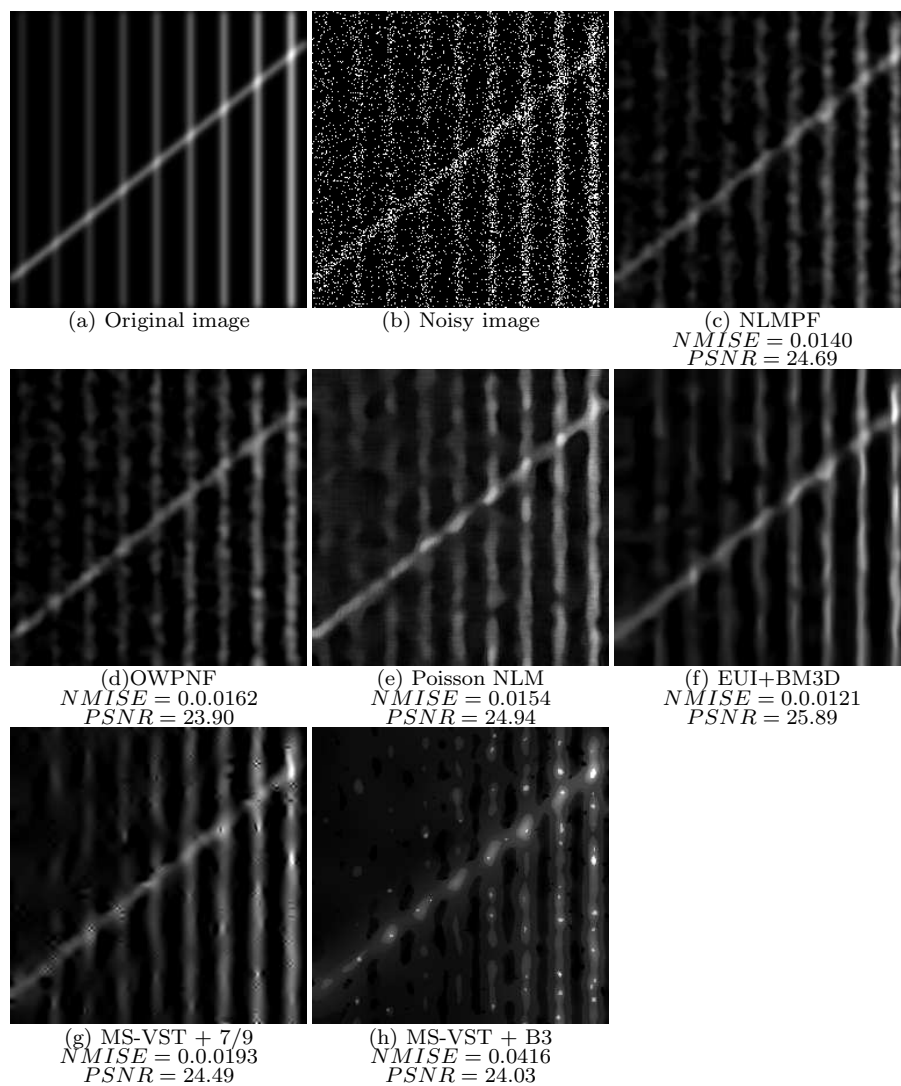


**Fig. 4** Poisson denoising of smooth ridges (image size:  $256 \times 256$ ). (a) intensity image (the peak intensities of the 9 vertical ridges vary progressively from 0.1 to 0.5; the inclined ridge has a maximum intensity of 0.3; background = 0.05); (b) Poisson noisy image; (c) NLMPF ( $M = 9 \times 9$ ,  $m = 21 \times 21$ ,  $d = 4$ ,  $\sigma_H = 0.5$ ,  $\mu = 0.4$ ,  $NMISE = 0.0140$ ); (d) Optimal Weights Filter ( $M = 9 \times 9$ ,  $m = 19 \times 19$ ,  $d = 3$  and  $H = 2$ ,  $NMISE = 0.0162$ ); (e) Poisson NLM ( $NMISE = 0.0154$ ); (f) Exact unbiased inverse + BM3D ( $NMISE = 0.0121$ ); (g) MS-VST + 7/9 biorthogonal wavelet ( $J = 5$ ,  $FPR = 0.001$ ,  $N_{max} = 5$  iterations,  $NMISE = 0.0193$ ); (h) MS-VST + B3 isotropic wavelet ( $J = 3$ ,  $FPR = 0.00001$ ,  $N_{max} = 10$  iterations,  $NMISE = 0.0416$ ).



**Fig. 5** Poisson denoising of the Barbara image (image size:  $256 \times 256$ ). (a) intensity image (intensity  $\in [0.93, 15.73]$ ); (b) Poisson noisy image; (c) NLMPF ( $M = 15 \times 15$ ,  $m = 21 \times 21$ ,  $d = 0$ ,  $\mu = 1$ ,  $NMISE = 0.1150$ ); (d) Optimal Weights Filter ( $M = 15 \times 15$ ,  $m = 21 \times 21$  and  $d = 0$ ,  $NMISE = 0.1061$ ); (e) Poisson NLM ( $NMISE = 0.1207$ ); (f) Exact unbiased inverse + BM3D ( $NMISE = 0.0863$ ) (h) MS-VST + 7/9 biorthogonal wavelet ( $J = 4$ ,  $FPR = 0.001$ ,  $N_{max} = 5$  iterations,  $NMISE = 0.2391$ ); (h) MS-VST + B3 isotropic wavelet ( $J = 5$ ,  $FPR = 0.001$ ,  $N_{max} = 5$  iterations,  $NMISE = 0.3777$ ).

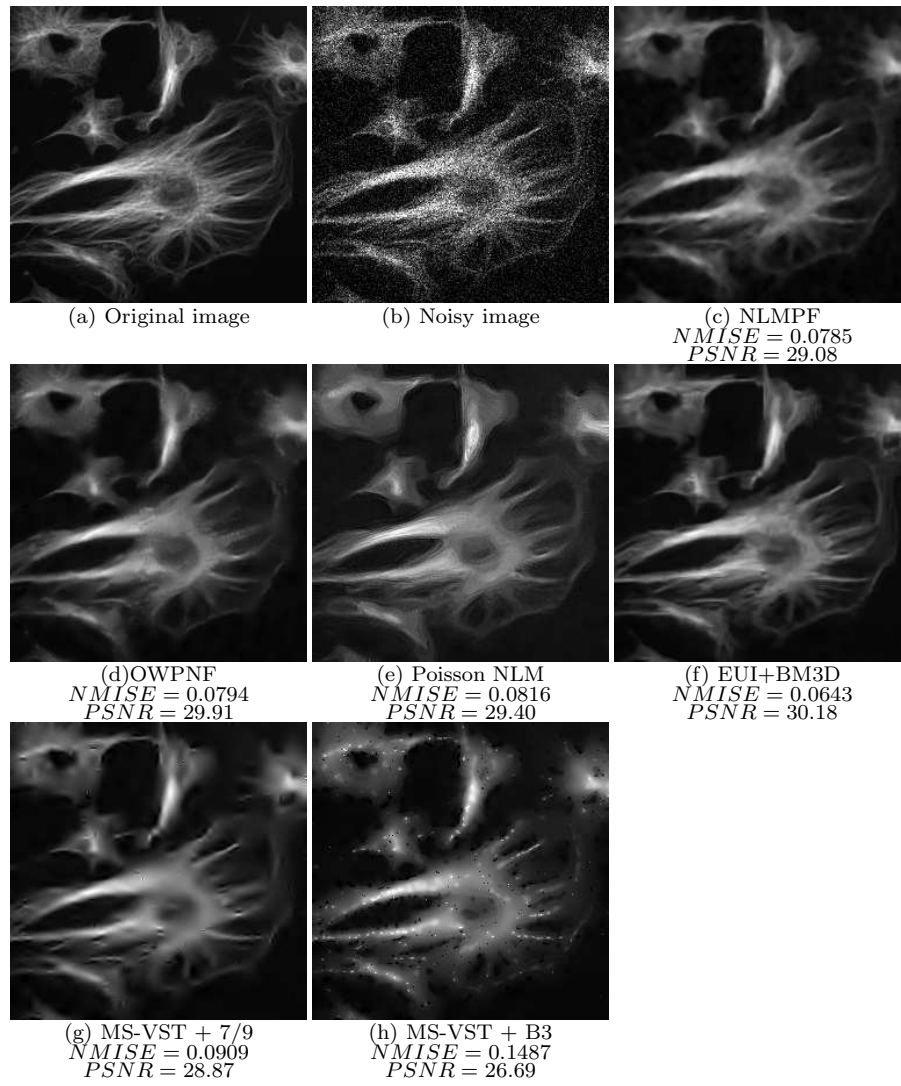


**Fig. 6** Poisson denoising of fluorescent tubules (image size:  $256 \times 256$ ). (a) intensity image (intensity  $\in [0.53, 16.93]$ ); (b) Poisson noisy image; (c) NLMPF ( $M = 7 \times 7$ ,  $m = 13 \times 13$ ,  $d = 2$ ,  $\sigma_H = 2$ ,  $\mu = 1$ ,  $NMISE = 0.0785$ ); (d) Optimal Weights Filter ( $M = 11 \times 11$ ,  $m = 17 \times 17$ ,  $d = 1$  and  $H = 0.6$ ,  $NMISE = 0.0794$ ); (e) Poisson NLM ( $NMISE = 0.0816$ ); (f) Exact unbiased inverse + BM3D ( $NMISE = 0.0643$ ) (g) MS-VST + 7/9 biorthogonal wavelet ( $J = 5$ ,  $FPR = 0.0001$ ,  $N_{max} = 5$  iterations,  $NMISE = 0.0909$ ); (h) MS-VST + B3 isotropic wavelet ( $J = 5$ ,  $FPR = 0.001$ ,  $N_{max} = 10$  iterations,  $NMISE = 0.1487$ ).